TRANSACTIONS OF THE
AMERICAN MATHEMATICAL SOCIETY
Volume 375, Number 12, December 2022, Pages 8399–8422
https://doi.org/10.1090/tran/8747
Article electronically published on October 3, 2022

SYMPLECTIC STRUCTURES WITH NON-ISOMORPHIC PRIMITIVE COHOMOLOGY ON OPEN 4-MANIFOLDS

MATTHEW GIBSON, LI-SHENG TSENG, AND STEFANO VIDUSSI

Abstract. We analyze four-dimensional symplectic manifolds of type $X = S^1 \times M^3$ where M^3 is an open 3-manifold admitting inequivalent fibrations leading to inequivalent symplectic structures on X. For the case where $M^3 \subset S^3$ is the complement of a 4-component link constructed by McMullen-Taubes, we provide a general algorithm for computing the monodromy of the fibrations explicitly. We use this algorithm to show that certain inequivalent symplectic structures are distinguished by the dimensions of the primitive cohomologies of differential forms on X. We also calculate the primitive cohomologies on X for a class of open 3-manifolds that are complements of a family of fibered graph links in S^3. In this case, we show that there exist pairs of symplectic forms on X, arising from either equivalent or inequivalent pairs of fibrations on the link complement, that have different dimensions of the primitive cohomologies.

1. Introduction

There is a well-known class of symplectic 4-manifolds that is intrinsically related to Riemann surfaces and its mapping class group. Given a finite type Riemann surface Σ and an element $f : \Sigma \to \Sigma$ of its mapping class group, we can combine the information of (Σ, f) into a three-dimensional manifold, the mapping torus $\pi : Y_f \to S^1$ with fiber Σ and monodromy given by f. We then take the product of Y_f with a circle S^1 and obtain a symplectic 4-manifold $X = S^1 \times Y_f$ whose symplectic structure can be constructed as follows (see Section 2 for more detail). Let $d\pi$ be the closed, non-degenerate 1-form associated to the projection map and dt the 1-form of the S^1 factor in X. Together with a global two-form ω_Σ of Y_f, which restricts to the volume form on each fiber, we can take the symplectic form to be $\omega_f = dt \wedge d\pi + \omega_\Sigma$. By construction, the data of this symplectic 4-manifold (X, ω_f) consists essentially of just (Σ, f).

Though simple in construction, this class of 4-manifolds has an interesting property. We recall that a three-dimensional manifold can have different fibrations with homeomorphic fibers, with the monodromy given by different elements of the mapping class group, or even fibrations with non-homeomorphic fibers. Of interest, the different fibrations would lead to different symplectic forms on X. It is therefore an interesting question whether symplectic forms from different fibrations are related or not in some particular way. In fact, it is known from the work of McMullen and Taubes [6] that the symplectic structures from different fibrations can be *inequivalent*. In this paper, following [6], we say that two symplectic forms (ω_0, ω_1)

Received by the editors May 26, 2021.
2020 *Mathematics Subject Classification.* Primary 57R57, 57K43, 57K20.
The second author was supported by the Simons Collaboration Grant No. 636284 and the third author was supported by the Simons Collaboration Grant No. 524230.

are *equivalent* if there is some combination of diffeomorphisms and smooth paths of symplectic forms interpolating between ω_0 and ω_1. Otherwise, we will call two symplectic forms *inequivalent*.

These 4-manifolds of course can be studied using tools from symplectic geometry. From this perspective, it is interesting to ask whether symplectic techniques on 4-manifolds can shed some light on the relationships between elements of the mapping class group of Riemann surfaces, in the case of different fibrations with homeomorphic fibers, and their associated symplectic structures. McMullen and Taubes used Seiberg-Witten invariants to demonstrate the inequivalence of two symplectic forms in their construction. Here, we will consider a more algebraic tool related to cohomologies of primitive differential forms introduced by Tseng and Yau [9].

In [9], Tseng-Yau studied a new cohomological invariant for any symplectic manifold (X, ω) denoted by $PH^*_{\pm}(X, \omega)$ (see also [8] for its underlying algebraic structure). Unlike the de Rham cohomology, the dimension of this symplectic cohomology is not an invariant of homeomorphism type and can depend on the symplectic structure. In fact, it was demonstrated explicitly in a 6-nilmanifold example that $PH^*_{\pm}(X, \omega)$ can jump in dimensions as the symplectic structure ω on X varies [9]. But prior to this work, as far as the authors are aware, no examples of dimension jumping were known for symplectic 4-manifolds. We will explain below how the dimensions of $PH^2_{\pm}(X, \omega)$ effectively count the number of Jordan blocks of size at least two in the decomposition of $f^* - 1 : H^1(\Sigma) \to H^1(\Sigma)$. This key fact together with our explicit calculations of the monodromy allows us to distinguish different symplectic structures on 4-manifolds of type $X = S^1 \times M^3$ arising from different fibrations for M^3. As a first example, inspired by the construction of McMullen and Taubes in [6], we find the following.

Theorem 1.1. *There exists a fibered 3-manifold M^3 admitting two different fibrations with monodromy f and g, yielding two associated symplectic structures on $X = S^1 \times M^3$ – (X, ω_f) and (X, ω_g) – that can be distinguished by the primitive cohomologies. In particular,*

$$\dim PH^2_+(X, \omega_f) \neq \dim PH^2_+(X, \omega_g).$$

The first example of inequivalent symplectic structures with distinct primitive cohomologies that we will describe in this paper is closely related to the construction of McMullen and Taubes where they showed the existence of a pair of inequivalent symplectic forms on a simply-connected 4-manifold starting from a 3-manifold M^3 that is a fibered link complement [6]. Their construction furnishes for us the fibration of M^3 with monodromy f referenced in Theorem 1.1. In [11], the third author found another fibration of M^3 with monodromy g whose associated symplectic structure is inequivalent from that associated with McMullen-Taubes' fibration. After carefully describing the monodromies f and g, we are able to show that the symplectic 4-manifolds (X, ω_f) and (X, ω_g) have distinct primitive cohomologies.

It turns out that our first example motivated by McMullen and Taubes is just the tip of the iceberg in terms of inequivalent symplectic structures having different primitive cohomologies. A large class of examples can be constructed from fibered 3-manifolds that are S^3 complements of graph links and studied in detail by Eisenbud

and Neumann [3]. In [10], the third author constructed a family of 3-manifolds, denoted by $M^{(2n)} = S^3 \backslash K^{(2n)}$ for any $n \in \mathbb{N}$, where $K^{(2n)} \subset S^3$ is a 2-component graph link. Its fibrations are encoded by a pair of integers (m_1, m_2) satisfying certain conditions. It was shown in [10] that the associated symplectic 4-manifold $X^{(n)} = S^1 \times M^{(2n)}$ admits at least $n+1$ inequivalent symplectic structures. We have investigated the primitive cohomology of this family of 4-manifolds and found that the dimension depends on the choice of the fibration (m_1, m_2), and in fact, directly relates to the divisibility of the m_i's by 3.

Theorem 1.2. *For $n \in \mathbb{N}$, let (m_1, m_2) be coprime, representing a fibration of the graph link $M^{(2n)} = S^3 \backslash K^{(2n)}$. By reversing the roles of m_1 and m_2 if necessary, we write $m_1 = 3^k q$ with $\gcd(q, 3) = 1$ and assume $\gcd(3, m_2) = 1$. Denote by $\omega_{(m_1,m_2)}$ the associated symplectic form on $X^{(n)} = S^1 \times M^{(2n)}$. The primitive cohomology is given by*

$$\dim PH_2^+(X^{(n)}, \omega_{(m_1,m_2)}) = \begin{cases} b_2(X^{(n)}) + 3^{n+k-\lceil \frac{k}{2} \rceil} - 3^k, & k \leq 2n-4, \\ b_2(X^{(n)}) + 2 \cdot 3^k, & 2n-3 \leq k \leq 2n-2, \\ b_2(X^{(n)}) + 1, & k \geq 2n-1, \end{cases}$$

where $b_2(X^{(n)}) = 3$ is the second Betti number.

These 4-manifolds associated with graph links not only have primitive cohomologies that may vary with the symplectic structures but also demonstrate other interesting properties worthy of further investigations. For instance, in addition to inequivalent symplectic structures possibly having different primitive cohomologies, we also found pairs of symplectic structures associated with *equivalent* 3-manifold fibrations having different primitive cohomologies as well. Similar to symplectic forms, we say for fibered 3-manifolds that two fibrations (π_0, π_1) of $M^3 \to S^1$ are *equivalent* if their corresponding one-forms $(d\pi_0, d\pi_1)$ are related by some combinations of diffeomorphisms and smooth paths of one-forms interpolating between them. Clearly, to distinguish equivalent versus inequivalent 3-manifold fibrations from the symplectic 4-manifold perspective would require more tools than just the dimension of the primitive cohomology. Regarding this, it may be helpful to point out that the differential forms underlying $PH^*(X, \omega)$ are situated in an A_3-algebra [8] and hence the cohomology has a ring structure and also Massey products different from those of $H^*(X)$. For the class of symplectic 4-manifolds $X = S^1 \times M^3$, where M^3 is the mapping torus with monodromy f, it would be insightful to relate the invariants coming from $PH^*(X, \omega_f)$ and all its products directly with the properties of the monodromy f as an element of the mapping class group. This can give a deeper link between the space of symplectic structures on X with the mapping class groups of Riemann surfaces and their corresponding mapping tori. This paper represents a significant first step in this direction focusing on the implications of the cohomology group.

The structure of the paper is as follows. In Section 2, we review the basic properties of $PH^*(X, \omega)$ and the de Rham cohomology of a fibered 3-manifold. In Section 3, we discuss the details of the McMullen-Taubes fibrations [6] and use their work and that of [11] to establish Theorem 1.1. The explanation of our calculations is given in Section 4 and the Appendix, where we provide the subtle details of our

explicit construction of the monodromy of the McMullen-Taubes surface bundle. In Section 5, we prove Theorem 1.2, where we investigate the symplectic structures and the primitive cohomologies of 4-manifolds constructed from the family of fibrations on graph links $K^{(2n)}$ introduced by the third author in [10]. These fibrations are determined by relatively prime pairs (m_1, m_2). Finally, we end in Section 6 with a discussion of our results.

2. Preliminaries

2.1. **de Rham and primitive cohomologies.** In this subsection, we briefly review the basics of the de Rham cohomology of surface bundles over a circle and also summarize the primitive cohomology studied in [8,9], applying it to symplectic 4-manifolds associated to surface bundles.

Let $\widehat{\Sigma}_g$ be a closed surface of genus g. We endow $\widehat{\Sigma}_g$ a symplectic structure, and we can assume, up to isotopy, that any self-diffeomorphism $\widehat{f}\colon \widehat{\Sigma}_g \to \widehat{\Sigma}_g$ preserves the symplectic form. Next, we consider the mapping torus of $\widehat{f}$, the closed 3-manifold $\widehat{Y}_{\widehat{f}} = \widehat{\Sigma}_g \times [0,1]/(x,1) \sim (\widehat{f}(x),0)$. It follows that $\widehat{Y}_{\widehat{f}}$ has a $\widehat{\Sigma}_g$-bundle structure over S^1 with the projection given by $\pi : \widehat{Y}_{\widehat{f}} \to S^1$, $\pi([x,t]) = t$. The associated map $\widehat{f}$ is called the *monodromy* of the bundle. We can endow the 4-manifold $S^1 \times \widehat{Y}_{\widehat{f}}$ with a symplectic structure by defining $\widehat{\omega} := dt \wedge d\pi + \widehat{\omega}_{\widehat{\Sigma}}$ where dt is the volume form on the S^1 factor and $\widehat{\omega}_{\widehat{\Sigma}}$ is a 2-form on $\widehat{Y}_{\widehat{f}}$ restricting to the volume form on $\widehat{\Sigma}$.

Let $\Sigma_{g,n} = \widehat{\Sigma}_g - \{y_1, \cdots, y_n\}$ be the surface of genus g with n points removed. When clear, the surface will simply be abbreviated by Σ. Moreover, when convenient, $P := \{y_1, \cdots, y_n\}$ may be thought of as marked points. The symplectic form on $\widehat{\Sigma}_g$ restricts to a symplectic form on Σ.

Let $\widehat{f}\colon \widehat{\Sigma}_g \to \widehat{\Sigma}_g$ be any symplectic diffeomorphism preserving P setwise. This restricts to a symplectic diffeomorphism $f\colon \Sigma \to \Sigma$. The 3-dimensional mapping torus $Y_f = \Sigma \times [0,1]/(x,1) \sim (f(x),0)$ is an open submanifold of $\widehat{Y}_{\widehat{f}}$, obtained by removing a collection of curves transverse to the fibers. Denoting, with slight abuse of notation, the new fibration by $\pi\colon Y_f \to S^1$ as well, its de Rham cohomology is determined by the Wang exact sequence

$$\cdots \longrightarrow H^0(\Sigma) \longrightarrow H^1(Y_f) \longrightarrow H^1(\Sigma) \xrightarrow{f^*-1} H^1(\Sigma) \longrightarrow H^2(Y_f) \longrightarrow \cdots.$$

This sequence yields

$$\begin{aligned} H^0(Y_f) &= \mathbb{R}, \\ H^1(Y_f) &= \ker(f^* - 1 : H^1(\Sigma) \to H^1(\Sigma)) \oplus \langle d\pi \rangle, \\ H^2(Y_f) &= \langle d\pi \rangle \wedge \operatorname{coker}(f^* - 1 : H^1(\Sigma) \to H^1(\Sigma)), \\ H^3(Y_f) &= 0. \end{aligned}$$

For $X = S^1 \times Y_f$, the restriction of the symplectic form on $S^1 \times \widehat{Y}_{\widehat{f}}$ to X yields the symplectic form $\omega = dt \wedge d\pi + \omega_\Sigma$, where ω_Σ (by abuse of notation) is a closed 2-form on Y_f that restricts to the symplectic form on each fiber. The Kunneth

formula also easily shows

$$\begin{aligned}
H^0(X) &= \mathbb{R},\\
H^1(X) &= \langle dt, d\pi\rangle \oplus \ker(f^* - 1 : H^1(\Sigma) \to H^1(\Sigma)),\\
H^2(X) &= \langle dt \wedge d\pi\rangle \oplus d\pi \wedge \operatorname{coker}(f^* - 1 : H^1(\Sigma) \to H^1(\Sigma))\\
&\qquad \oplus dt \wedge \ker(f^* - 1 : H^1(\Sigma) \to H^1(\Sigma)),\\
H^3(X) &= \langle dt \wedge d\pi\rangle \wedge \operatorname{coker}(f^* - 1 : H^1(\Sigma) \to H^1(\Sigma)),\\
H^4(X) &= 0.
\end{aligned}$$

We now turn to describing the primitive cohomology on the symplectic 4-manifold. Given a symplectic manifold (X^{2n}, ω), choose a basis $\{\partial_{x^i}\}_{i=1}^{2n}$ for TX. Its differential forms $\Omega^*(X)$ carry an $sl_2(\mathbb{R})$ action, with the following sl_2-representation:

$$\begin{aligned}
L : \Omega^k(X) &\to \Omega^{k+2}(X),\\
A_k &\mapsto \omega \wedge A_k,
\end{aligned}$$

$$\begin{aligned}
\Lambda : \Omega^k(X) &\to \Omega^{k-2}(X),\\
A_k &\mapsto \frac{1}{2}(\omega^{-1})^{ij}\iota_{\partial_{x^i}}\iota_{\partial_{xj}}A_k,
\end{aligned}$$

$$\begin{aligned}
H : \Omega^k(X) &\to \Omega^k(X),\\
A_k &\mapsto (n-k)A_k
\end{aligned}$$

with $[H, \Lambda] = 2\Lambda$, $[H, L] = -2L$, and $[\Lambda, L] = H$.

The *primitive forms* $\mathcal{P}^*(X)$ are the highest weight vectors in this algebra. That is, $A_k \in \mathcal{P}^k(X)$ precisely if $\Lambda A_k = 0 = \omega^{n-k+1} \wedge A_k$. This action leads to the Lefschetz decomposition so that any k-form has an expression $A_k = B_k + \omega \wedge B_{k-2} + \omega^2 \wedge B_{k-4} + \cdots$ where each B_i is primitive. In [9], Tseng and Yau constructed the differentials $\partial_\pm : \mathcal{P}(X)^k \to \mathcal{P}^{k\pm1}(X)$ and the elliptic complex

$$\begin{array}{ccccccccccccc}
0 & \longrightarrow & \mathcal{P}^0 & \xrightarrow{\partial_+} & \mathcal{P}^1 & \xrightarrow{\partial_+} & \mathcal{P}^2 & \xrightarrow{\partial_+} & \cdots & \xrightarrow{\partial_+} & \mathcal{P}^n & & \\
 & & & & & & & & & & \downarrow{\scriptstyle \partial_+\partial_-} & & \\
0 & \xleftarrow{\partial_-} & \mathcal{P}^0 & \xleftarrow{\partial_-} & \mathcal{P}^1 & \xleftarrow{\partial_-} & \mathcal{P}^2 & \xleftarrow{\partial_-} & \cdots & \xleftarrow{\partial_-} & \mathcal{P}^n & &
\end{array}$$

whose "top" and "bottom" cohomologies are denoted $PH^*_+(X, \omega)$ and $PH^*_-(X, \omega)$, respectively. Also in [8], it is proven that certain de Rham cohomological data is enough to compute the symplectic cohomology groups $PH^*_\pm(X)$, given by the isomorphisms below for $k \le n$:

(2.1)
$$\begin{aligned}
PH^k_+(X) &\cong \operatorname{coker}(L : H^{k-2}(X) \to H^k(X)) \oplus \ker(L : H^{k-1}(X) \to H^{k+1}(X)),\\
PH^k_-(X) &\cong \operatorname{coker}(L : H^{2n-k-1}(X) \to H^{2n-k+1}(X)) \oplus ker(L : H^{2n-k}(X)\\
&\qquad \to H^{2n-k+2}(X)).
\end{aligned} \tag{2.2}$$

Let us first discuss the case where ω is chosen so that $[\omega]_{dR} = [dt \wedge d\pi]_{dR}$, the more general case will be treated at the end of the section. Applying equations (2.1)

and (2.2) to the 4-manifold $X = S^1 \times Y_f$, along with computations from earlier in this section, yields

$$\begin{aligned}
&PH^0_+(X) \cong \mathbb{R},\\
&PH^1_+(X) \cong H^1(X),\\
&PH^2_+(X) \cong H^2(X)/\langle dt \wedge d\pi\rangle \oplus \langle dt, d\pi\rangle \oplus [\ker(f^* - 1) \cap \operatorname{Im}(f^* - 1)],\\
&PH^2_-(X) \cong H^2(X) \oplus [\langle dt \wedge d\pi\rangle \wedge \operatorname{coker}(f^* - 1)] \,/\, [\langle dt \wedge d\pi\rangle \wedge \ker(f^* - 1)]\,,\\
&PH^1_-(X) \cong H^3(X),\\
&PH^0_-(X) \cong 0.
\end{aligned}$$

Let b_i denote the Betti numbers of X and $p_i^{\pm}(X, \omega)$ denote the dimensions of $PH^i_{\pm}(X, \omega)$. When the choice of the underlying symplectic structure is clear, we simply write $p_i^{\pm}$. Then,

$$\begin{aligned}
p_0^+ &= 1,\\
p_1^+ &= b_1,\\
p_2^+ &= b_2 + 1 + \dim\left[\ker(f^* - 1) \cap \operatorname{Im}(f^* - 1)\right],\\
p_2^- &= b_2 + \dim\left[\ker(f^* - 1) \cap \operatorname{Im}(f^* - 1)\right],\\
p_1^- &= b_3,\\
p_0^- &= 0,
\end{aligned}$$

where we have used the fact that $\dim\left[\ker(f^* - 1) \cap \operatorname{Im}(f^* - 1)\right]$ and

$$\dim\left[(dt \wedge d\pi \wedge \operatorname{coker}(f^* - 1))/(dt \wedge d\pi \wedge \ker(f^* - 1))\right]$$

are equal by realizing that both quantities count the number of Jordan blocks of $f^* - 1$ of size strictly greater than 1 (see discussion below). We note that the *primitive Euler characteristic* $\chi_p(X) = \sum(-1)^i p_i^+ - \sum(-1)^i p_i^- = 2 - b_1 + b_3$ is fixed under homeomorphism type. However, the primitive Betti numbers $p_2^{\pm}$ may vary in general.

Let us explain how this dimension relates to the Jordan blocks of $f^* - 1$. For brevity we write $\nu_2 := \dim\left[\ker(f^* - 1) \cap \operatorname{Im}(f^* - 1)\right]$. Now, if $\alpha \in \ker(f^* - 1) \cap \operatorname{Im}(f^* - 1)$, then $(f^* - 1)\alpha = 0$ and $(f^* - 1)\beta = \alpha$ for some β. That is, α is an eigenvector in a Jordan chain of length at least 2. It follows that ν_2 counts the number of Jordan blocks corresponding to eigenvalue $\lambda = 1$ of size *at least* 2. More generally, there is a descending filtration of subgroups $PH^2_+(M) \supset J_1(M) \supset J_2(M) \supset \cdots$ where $J_k(M) = \ker(f^* - 1) \cap \operatorname{Im}(f^* - 1)^k$. If $\alpha \in J_k(M)$, then it is the eigenvector in a Jordan chain of length at least $k + 1$ given by $x_1 = \alpha$, $x_2 = (f^* - 1)^{k-1}\beta$, $x_3 = (f^* - 1)^{k-2}\beta$, $\cdots$, $x_k = (f^* - 1)\beta$, $x_{k+1} = \beta$. Thus, the dimension of the filtered quotient J_{k-1}/J_k counts the number of Jordan blocks of size *exactly* k.

In general, it is also possible to consider other symplectic structures on $X = S^1 \times Y_f$ where $[\omega] \neq [dt \wedge d\pi]$. Though not our main focus, we will describe how a different choice of the symplectic structure would affect the calculation of the primitive cohomology in the remainder of this subsection. To begin, let $i : \Sigma \hookrightarrow Y_f$ be the inclusion map of the fiber and choose $\tilde{\omega}_f \in \Omega^2(Y_f)$ such that $i^*(\tilde{\omega}_f) = \omega_\Sigma$. Furthermore, assume $\tilde{\omega}_f$ can be chosen so that $[\omega_0] := [dt \wedge d\pi + \tilde{\omega}_f] = [dt \wedge d\pi]$. Then $PH^*(X, \omega_0)$ is given by the above computations. Now, given any 1-form

$\eta \in \Omega^1(Y_f)$ such that $d(\eta \wedge d\pi) = 0$, we can define a new symplectic form, $\omega_\eta := \omega_0 + \eta \wedge d\pi = (dt + \eta) \wedge d\pi + \tilde{\omega}_f$. Of interest are those η's such that $[\omega_\eta] \neq [\omega_0]$, which occurs precisely when $[d\pi \wedge \eta] \in H^2(Y_f)$ is non-trivial. Choose a Jordan basis $\{x_{i,0}\}_{i=1}^k$ for $\ker(f^* - 1)$ and denote the corresponding Jordan chain of $x_{i,0}$ by $\{x_{i,0}, x_{i,1}, \cdots, x_{i,n_i}\}$. Rearranging if necessary, we assume $n_i = 0$ for $1 \leq i \leq s$. Thus $\{x_{i,0}\}_{i=1}^s$ are the Jordan blocks of size exactly 1. Then, we can write

$$H^1(Y_f) = \langle d\pi \rangle \oplus \langle x_{i,0} \rangle_{i=1}^k,$$
$$H^2(Y_f) = \langle d\pi \wedge x_{i,n_i} \rangle_{i=1}^k,$$

and express $[d\pi \wedge \eta] = \sum_{i=1}^k \lambda_i [d\pi \wedge x_{i,n_i}]$. We may write

$$PH^2_+(X, \omega_\eta) = H^2(X)/\langle [\omega_\eta] \rangle \oplus K_\eta$$

where $K_\eta = \ker(\omega_\eta \wedge : H^1(X) \to H^3(X))$. Then

$$[\omega_\eta \wedge d\pi] = [0],$$
$$[\omega_\eta \wedge dt] = [\eta \wedge d\pi \wedge dt] = -[dt \wedge d\pi \wedge \eta],$$
$$[\omega_\eta \wedge x_{i,0}] = [dt \wedge d\pi \wedge x_{i,0}].$$

We see that $[\omega_\eta \wedge (\sum_{i=1}^s \lambda_i x_{i,0} + dt)] = [dt \wedge d\pi \wedge \sum_{i=s+1}^k \lambda_i x_{i,n_i}]$, which is trivial if and only if $\eta \in \ker(f^* - 1)$. Similarly, denote by $C_\eta = \operatorname{coker}(\omega_\eta \wedge : H^1(X) \to H^3(X))$. The above computations show $C_\eta \cong \langle dt \wedge d\pi \wedge x_{i,n_i} \rangle_{i=s+1}^k / \langle dt \wedge d\pi \wedge \eta \rangle$. The quotient by the η term will be extraneous in the case that $\eta \in \ker(f^* - 1)$. In all, the resulting primitive cohomology groups $PH^*(X, \omega_\eta)$ can be expressed as follows.

$$PH^0_+(X, \omega_\eta) \cong H^0(X),$$
$$PH^1_+(X, \omega_\eta) \cong H^1(X),$$
$$PH^2_+(X, \omega_\eta) \cong H^2(X)/\langle [\omega_\eta] \rangle \oplus K_\eta,$$
$$PH^2_-(X, \omega_\eta) \cong H^2(X) \oplus C_\eta,$$
$$PH^1_-(X, \omega_\eta) \cong H^3(X),$$
$$PH^0_-(X, \omega_\eta) \cong \langle 0 \rangle,$$

where

$$K_\eta \cong \begin{cases} \langle d\pi \rangle \oplus \langle x_{i,0} \rangle_{i=s+1}^k, & \lambda_i \neq 0 \text{ for some } i > s, \\ \langle d\pi, dt + \eta \rangle \oplus \langle x_{i,0} \rangle_{i=s+1}^k, & \lambda_i = 0 \text{ for all } i > s, \end{cases}$$

$$C_\eta \cong \begin{cases} \langle dt \wedge d\pi \wedge x_{i,n_i} \rangle_{i=s+1}^k / \langle dt \wedge d\pi \wedge \eta \rangle, & \lambda_i \neq 0 \text{ for some } i > s, \\ \langle dt \wedge d\pi \wedge x_{i,n_i} \rangle_{i=s+1}^k, & \lambda_i = 0 \text{ for all } i > s. \end{cases}$$

Regardless of the class of η, we see $PH^k_\pm(X, \omega_\eta)$ are isomorphic to de Rham cohomologies for $k = 0, 1$. Furthermore, in the case that η descends to a cohomology class $[\eta] \in H^1(Y_f)$, the above computations show $\dim PH^*(X, \omega_\eta) = \dim PH^*(X, \omega_0)$. Unless otherwise stated, in the remainder of the paper, we assume $[\omega] = [dt \wedge d\pi]$.

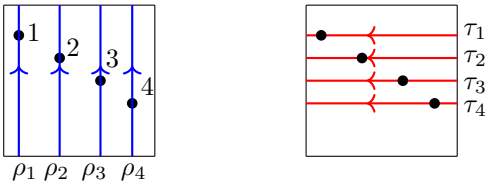

FIGURE 1. ρ_i and τ_i paths on $\Sigma_{1,4}$

2.2. **Mapping class group.** In this subsection, we review some of the necessary topics relevant to our work from mapping class group theory. We focus mainly on the mapping class group of $\Sigma_{1,4}$, detailing a set of generators described by Birman in [1]. We wish to study the diffeomorphisms of $\Sigma_{g,n}$ up to an equivalence. We define the *mapping class group*, denoted by $\mathcal{M}(\Sigma_{g,n})$, as the group of diffeomorphisms fixing P setwise, up to isotopies fixing P setwise. We define the *pure mapping class group*, $\mathcal{PM}(\Sigma_{g,n})$, as the subset of elements from $\mathcal{M}(\Sigma_{g,n})$ fixing P pointwise. Since the majority of this paper takes place in $\mathcal{PM}(\Sigma_{1,4})$ we briefly discuss the diffeomorphisms generating this subgroup for the torus with four marked points. We define τ_i as the longitudinal curve which passes above $y_1, y_2, \cdots, y_{i-1}$, through y_i, and below $y_{i+1}, \cdots, y_n$. Denote by ρ_i the meridian curve passing through y_i.

From these curves we define homeomorphisms $\mathcal{P}ush(\tau_i)$ and $\mathcal{P}ush(\rho_i)$, called the point-pushing maps. These are classical maps in mapping class group theory. They may be loosely visualized as follows: $\mathcal{P}ush(\tau_i)$ is the map which pushes the point x_i around the curve τ_i, "dragging" the rest of the surface $\Sigma_{1,4}$ with it. $\mathcal{P}ush(\rho_i)$ has a similar interpretation. In [1], Birman showed that the push maps generate the mapping class group:

$$\mathcal{PM}(\Sigma_{1,4}) = \langle \mathcal{P}ush(\tau_i), \mathcal{P}ush(\rho_i) \rangle, i = 1, 2, 3, 4.$$

It turns out that these maps can be realized in terms of Dehn twists along homology generators for $H_1(\Sigma_{1,4})$. These explicit expressions are worked out in the Appendix. (The curves ρ_i and τ_i are pictured in Figure 1, drawn on the square representing $\Sigma_{1,4}$.)

Another important subgroup of the mapping class group is the *Torelli group*, $\mathcal{I}(\Sigma)$, consisting of diffeomorphisms acting trivially on (co)homology. Thus,

$$\mathcal{I}(\Sigma) = \{f \in \mathcal{M}(\Sigma) : 1 = f^* : H^1(\Sigma) \to H^1(\Sigma)\}.$$

Calculations in Section 2.2 show that if $f \in \mathcal{I}(\Sigma)$, then $H^*(S^1 \times Y_f) = H^*(T^2 \times \Sigma)$ and $PH^*(S^1 \times Y_f) = PH^*(T^2 \times \Sigma)$ as groups. Thus two Torelli-bundles cannot be distinguished from their primitive cohomology groups alone. However, by the same reasoning, $f \in \mathcal{I}$ and $g \notin \mathcal{I}$ can *always* be distinguished by the dimension of the cohomology groups.

3. McMullen-Taubes type 4-manifolds

In this section, we will discuss different presentations of a 3–manifold, the complement of a link in S^3, as fibration with fiber a punctured torus or sphere. All the torus fiber examples will induce symplectic structures with identical primitive cohomologies but the sphere fibration will be shown to give primitive cohomology of different dimension.

TABLE 1. Monodromies

Type	Projection Vector v_1	Monodromy
Spherical	(0,0,0,1)	$\sigma_1^{-1}\sigma_2\sigma_1^{-1}\sigma_2\sigma_1^{-1}\sigma_2$
Toroidal	$(-1,-1,1)$	$\tau_3^{-1}\tau_2^{-1}\tau_1^{-1}\rho_1^{-1}\rho_2^{-1}\tau_1^{-1}\rho_2\tau_4^{-1}\rho_4^{-1}\tau_3^{-1}$
Toroidal	$(-1,1,1)$	$\rho_2^{-1}\tau_1\rho_2^{-1}\tau_1^{-1}\tau_4^{-1}\rho_3^{-2}\tau_2^{-1}\rho_4^{-1}\rho_1^{-1}$

We quickly review the examples constructed in [6] and [11]. In [6], McMullen and Taubes considered a 3-manifold M which is a link complement $S^3\backslash K$. Here, K is the Borromean rings $K_1 \cup K_2 \cup K_3$ plus K_4, the axis of symmetry of the rings. By performing 0-surgery along the Borromean rings we obtain a presentation of M as $\mathbb{T}^3\backslash L$ where:

- $L \subset \mathbb{T}^3$ is a union of four disjoint, closed geodesics L_1, L_2, L_3, L_4,
- $H_1(\mathbb{T}^3) = \langle L_1, L_2.L_3\rangle$,
- $L_4 = L_1 + L_2 + L_3$.

The fiber of M is the 2-torus with punctures coming from the L_i. The different fibration structures are captured by the Thurston ball. In [6], this ball is computed as the dual of the Newton polytope of the Alexander polynomial. Endow the ball with coordinates $\phi = (x, y, z, t)$ as in [6]. Then, the Thurston unit ball has 16 top–dimensional faces (each fibered) coming in 8 pairs under the symmetry $(\phi, -\phi)$. Furthermore, restricting to faces that are dual to those vertices of the Newton polytope with no t–component, we get 14 faces that come in two types; quadrilateral and triangular. It is shown in [6] that there exists a pair of inequivalent symplectic forms on a 4-manifold coming from different fibrations of $\mathbb{T}^3\backslash L$. These fibrations correspond to points lying on the two distinct types of faces. In [11], it is shown that the remaining pair of $16 - 14 = 2$ faces (with a non-zero t-component) yields a third symplectic structure which is inequivalent to the two found by McMullen and Taubes.

We will investigate the monodromy of the fibration given in [11], in which it is observed that M admits a fibration with fiber the four-punctured 2-sphere. Table 1 summarizes the conclusions of the examples to follow. Determining these monodromy formulas explicitly is a crucial step in computing the dimension of $PH^2_{\pm}(X, \omega)$, since it depends on the Jordan decomposition.

The first example is the fibration with fiber $\Sigma_{0,4}$, hence 'spherical' type. The other two examples are of 'toroidal' type with fiber $\Sigma_{1,4}$. In the spherical example, the given projection vector is the cohomology class in $H^1(M^3)$ corresponding to a point on the Thurston ball. The projection vectors of the 'toroidal' type examples refer to the vector used in its fiber bundle construction and not the point on the Thurston ball. These details are elaborated on in the Appendix. For notational simplicity, in Table 1, $\mathcal{P}ush(\rho_i)$ and $\mathcal{P}ush(\tau_i)$ are abbreviated to ρ_i and τ_i, respectively.

Spherical example. In this example, we take the fibration from [11] obtained by performing 0-surgery along the K_4 axis. The fiber is S^2 punctured four-times, with monodromy given by the braid word corresponding to the Borromean rings. Let σ_i denote the half-Dehn twist which switches marked points i and $i + 1$. This homeomorphism can be viewed similar to the push map, where we "push" the surface through the arc connecting the ith and $(i + 1)$th points. As a braid, it

is the element which passes the ith string over the $(i+1)$th string. Under this identification, the monodromy is given by

$$\sigma_1^{-1}\sigma_2\sigma_1^{-1}\sigma_2\sigma_1^{-1}\sigma_2.$$

The derivation of the toroidal type monodromies is much more involved. We carefully work out these formulas in the next section. For now, we take the monodromies from Table 1 as true and examine their cohomological implications.

Cohomological analysis. Denote by g the monodromy from fiber the four-punctured 2-sphere $\Sigma_{0,4}$. Similarly, f denotes either of the two monodromies coming from the four–punctured torus fiber $\Sigma_{1,4}$ in Table 1. With the monodromy f, we can compute its action on $H^1(\Sigma_{1,4})$ (either by hand or with the help of software) to conclude that $\dim\ker(f^*-1) = b_1(Y_f) - 1 = 3$ in both 'toroidal' cases. Let $X = S^1 \times Y_f = S^1 \times Y_g$, these manifolds being diffeomorphic by the above discussion. We will compute the primitive cohomology of the symplectic structures associated to the fibrations determined by the monodromies f and g.

With respect to the ordering $(a_0, a_1, a_2, a_3, b_0)$ of basis vectors for $H^1(\Sigma_{1,4})$, computation shows the action on $H^1(\Sigma_{1,4})$ is given by

$$f^*-1 = \begin{pmatrix} -1 & -1 & -1 & -1 & 1 \\ 0 & 0 & 0 & 0 & -1 \\ 1 & 1 & 1 & 1 & 1 \\ 0 & 0 & 0 & 0 & -1 \\ 0 & 0 & 0 & 0 & 0 \end{pmatrix}, \qquad J = \begin{pmatrix} 0 & 1 & 0 & 0 & 0 \\ 0 & 0 & 0 & 0 & 0 \\ 0 & 0 & 0 & 1 & 0 \\ 0 & 0 & 0 & 0 & 0 \\ 0 & 0 & 0 & 0 & 0 \end{pmatrix},$$

for all f. Here J is the Jordan matrix for f^*-1. We note it has two blocks of size 2 and one of size 1. It follows that

$$\begin{aligned} \ker(f^*-1) &= \langle (1,0,0,-1,0), (0,1,0,-1,0), (0,0,1,-1,0)\rangle, \\ \operatorname{Im}(f^*-1) &= \langle (-1,0,1,0,0), (1,-1,1,-1,0)\rangle. \end{aligned}$$

A quick check shows

$$(f^*-1)(-1,0,1,0,0) = 0 = (f^*-1)(1,-1,1,-1,0).$$

Hence, we conclude

$$\dim\ker(f^*-1) \cap \operatorname{Im}(f^*-1) = \dim\operatorname{Im}(f^*-1) = 2.$$

Notice this dimension agrees with the number of blocks from J of size at least 2. Computations from Section 2.1 show that for any choice of η associated to ω_f we have either

$$p_2^+(X,\omega_f) = \begin{cases} 9, & \eta \text{ is such that } \lambda_i \neq 0 \text{ for some } i > s, \\ 10, & \eta \text{ is such that } \lambda_i = 0 \text{ for all } i > s. \end{cases}$$

We now turn to (X, ω_g). Since Y_f is diffeomorphic to Y_g, we must have

$$\dim\ker(g^*-1) = \dim\ker(f^*-1) = 3.$$

Moreover, using the formula $\chi(\Sigma_{g,n}) = 2-2g-n$, it follows $\chi(\Sigma_{0,4}) = -2 = 1 - b_1(\Sigma_{0,4})$, and so $b_1(\Sigma_{0,4}) = 3$. But by Rank-Nullity, $3 = 3 + \dim\operatorname{Im}(g^*-1)$, from which it follows $\dim\ker(g^*-1) \cap \operatorname{Im}(g^*-1) = 0$. Thus $p_2^+(X,\omega_g) = b_2(X_g) + 1 = 8 \neq p_2^+(X,\omega_f)$.

We point out that from the Jordan form of the f, these monodromies are not Torelli elements of $\mathcal{M}(\Sigma_{1,4})$. However, by dimension considerations, we saw $\dim \mathrm{Im}(g^* - 1) = 0$ and so g *is* a Torelli element of $\mathcal{M}(\Sigma_{0,4})$. Moreover, even though each f, f' coming from fiber $\Sigma_{1,4}$ are not Torelli, $f^* = f'^*$ and so it follows that $f'f^{-1}$ is a Torelli element.

These calculations give Theorem 3.1.

Theorem 3.1. *There exist inequivalent fibrations of the* 3*-manifold* M *with inequivalent associated symplectic* 4*-manifolds* (X, ω_f), (X, ω_g), *which can be distinguished by primitive cohomologies. In particular,*

$$p_2^+(X, \omega_f) \neq p_2^+(X, \omega_g).$$

To establish Theorem 3.1, it only remains to verify the toroidal type monodromies in Table 1. Before this verification, we point out an interesting feature of p_2^+ in this situation. By calculations from Section 2, $p_2^+(X, \omega_h) = 8 + \dim \ker(h^* - 1) \cap \mathrm{Im}(h^* - 1) \geq 8$ for *any* monodromy h. However, if h is some monodromy on $\Sigma_{1,4}$ we know its Jordan decomposition must give blocks of size $(2, 2, 1)$ or $(3, 1, 1)$. That is, h has at least one block of size of at least 2, so that $p_2^+ > 8$. Consequently, p_2^+ can distinguish the monodromy type in the sense that $p_2^+(X, \omega_f)$ is always larger than $p_2^+(X, \omega_g)$ for any $f \in \mathcal{M}(\Sigma_{1,4})$ and $g \in \mathcal{M}(\Sigma_{0,4})$. Moreover, the toroidal type examples above all have block sizes $(2, 2, 1)$. But if a monodromy with sizes $(3, 1, 1)$ existed, p_2^+ could also distinguish the two. Nonetheless, the exploration of the explicit constructions of the McMullen-Taubes type monodromies is still valuable. It provides an algorithm to produce the concrete Dehn twists which are responsible for the actions of $f^* - 1$ on cohomology.

4. Construction of monodromies

In this section, we provide details for the construction of the toroidal monodromies in Table 1. The Appendix gives an even more specific outline of the procedure that follows. In the examples to come, we take different bases $v_1 = (a_1, a_2, a_3)$, $v_2 = (1, 1, 0)$, $v_3 = (0, 1, 1)$ and fiber along v_1 so that the fiber at time t looks like $\Sigma_{t,4} = tv_1 + \langle v_2, v_3 \rangle$ with marked points

$$\begin{aligned} y_1(t) &= (-4\epsilon, 3\epsilon) + (a_3 - a_2, -a_3)t, \\ y_2(t) &= (-\epsilon, 2\epsilon) + (-a_1, a_1 - a_2)t, \\ y_3(t) &= (0, 0) + (a_3 - a_2, a_1 - a_2)t, \\ y_4(t) &= (\epsilon, -3\epsilon) + (-a_1, -a_3)t. \end{aligned}$$

Here, ϵ is some small fixed constant used to shift the marked points away from the origin at $t = 0$. The vector v_1 is the projection vector given in column 2 of Table 1. The general idea is as follows,

(1) Using the paths of the punctures y_i, find relative locations to determine if y_i passes above or below y_j.
(2) Express $\mathcal{P}ush(y_i(t))$ of the y_i path in terms of generators $\mathcal{P}ush(\rho_i)$, $\mathcal{P}ush(\tau_i)$.
(3) Calculate the intersection points of punctures $(y_i(t), y_j(t))$ at times (t_i, t_j). If $t_i > t_j$ then y_i crosses over y_j. If $t_i < t_j$ then y_j crosses over y_i.

(4) Use the crossings information to determine the order of $\mathcal{P}ush(y_i(t))$ maps in the final monodromy.

The procedure is best demonstrated through examples. As before, we drop the push notation so that $\mathcal{P}ush(\rho_2)\mathcal{P}ush(\tau_1)^{-1}\mathcal{P}ush(\tau_3)$ is simply denoted by $\rho_2\tau_1^{-1}\tau_3$. We also use function notation right to left so that the previous word indicates y_3 travels along τ_3 then y_1 along the inverse of τ_1 then finally y_2 along ρ_2. Homeomorphism type of the below examples was confirmed with SnapPy [2].

Toroidal example 1. $v_1 = (-1, -1, 1)$.

The paths of the corresponding marked points are

$$\begin{aligned} y_1(t) &= (-4\epsilon, 3\epsilon) + (2, -1)t, \\ y_2(t) &= (-\epsilon, 2\epsilon) + (1, 0)t, \\ y_3(t) &= (0, 0) + (2, 0)t, \\ y_4(t) &= (\epsilon, -3\epsilon) + (1, -1)t. \end{aligned}$$

Thus y_2 and y_3 travel in a parallel horizontal direction. y_1 and y_4 travel downwards and to the right and so will intersect both y_2 and y_3. We first find these intersection times. We illustrate the process for y_1 and y_3 and summarize the other points in Table 2. We need times t_1 and t_3 so that $y_1(t_1) = y_3(t_3)$. In other words, we seek a solution to the system

$$\begin{aligned} -4\epsilon + 2t_1 &= 2t_3, \\ 3\epsilon - t_1 &= 0, \end{aligned}$$

which gives $(t_1, t_3) = (3\epsilon, \epsilon + \frac{n}{2})$, $n = 0, 1$. Hence y_1 and y_3 intersect twice. The first time y_1 passes over y_3. Then at $t_3 = \epsilon + \frac{1}{2}$, y_3 crosses y_1. At $t_2 = \frac{5}{8}\epsilon + \frac{1}{2}$, y_2 passes over y_1. Similarly solving the corresponding system for y_2 and y_3 yields $(t_2, t_3) = (\frac{2}{3}\epsilon + \frac{n}{2}, 1 - \frac{1}{3}\epsilon)$, $n = 0, 1$. Both y_2 times occur before y_3, hence we conclude y_3 passes over y_2 twice. The remaining points of intersection are given in Table 2. The times specified are the later of the two crossing times and the points have been listed in order of intersection occurrence, from first to last.

TABLE 2. Toroidal example 1 intersections

Points	Time	Crossing
(y_1, y_3)	3ϵ	y_1 over y_3
(y_1, y_3)	$\epsilon + \frac{1}{2}$	y_3 over y_1
(y_2, y_4)	$1 - 3\epsilon$	y_2 over y_4
(y_3, y_4)	$1 - 3\epsilon$	y_4 over y_3
(y_1, y_2)	$1 - \epsilon$	y_2 over y_1
(y_1, y_4)	$1 - \epsilon$	y_1 over y_4
(y_3, y_4)	$1 - \epsilon$	y_3 over y_4

Pictured in Figure 1 are the paths of the y_i drawn in the plane (up to identification), where we have decomposed the "diagonal" paths of y_1 and y_4 into a combination of basis curves ρ_i and τ_i. To find the path of y_1, for example, we must use its velocity vector $(2, -1)$ as well as the relative locations of y_1 with respect to the start points of y_2, y_3, and y_4. Given that point y_2 starts at $(-\epsilon, 2\epsilon)$, we have

$y_1(\frac{3}{2}\epsilon) = (-\epsilon, \frac{3}{2}\epsilon)$ and so y_1 travels 'below' the y_2 start point. Similar computations show y_1 travels above both the y_3 and y_4 start points. As illustrated in Figure 1, the velocity vector $(2, -1)$ suggests y_1 has a path given by $\tau_1^{-1}\rho_1^{-1}\tau_1^{-1}$. However the diagonal path homotopic to this combination will not preserve the condition that y_1 travels below the y_2 start point. To remedy this situation, we must begin the y_1 monodromy with the loop C_{12}. This curve travels counterclockwise from y_1, enclosing y_2. Figure 1 illustrates the $\tau_1^{-1}C_{12}$ portion of the monodromy.

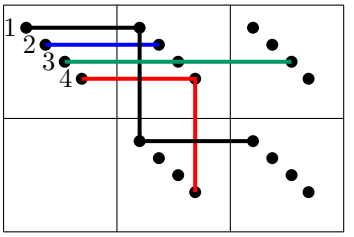

FIGURE 2. Example 1 marked point paths

y_4 is the only other diagonal path. We can easily check that it travels above the y_1, y_2, and y_3 start points. Hence its path is simply given by $\tau_4^{-1}\rho_4^{-1}$, indicated by the $(1, -1)$ velocity vector.

Summarizing, the monodromies of the punctures are given by

$$\begin{aligned} y_1(t) &: \tau_1^{-1}\rho_1^{-1}\tau_1^{-1}C_{12} = \tau_1^{-1}\rho_1^{-1}\rho_2^{-1}\tau_1^{-1}\rho_2, \\ y_2(t) &: \tau_2^{-1}, \\ y_3(t) &: \tau_3^{-2}, \\ y_4(t) &: \tau_4^{-1}\rho_4^{-1}. \end{aligned}$$

Now, we must determine the order of these individual monodromies in the final map. Using the above formulas, it's clear $y_2(t)$ and $y_3(t)$ are parallel so their relative order to each other in the final monodromy doesn't matter. From Table 1, we see every other point crosses over y_3 first, but then y_3 crosses over y_1 and y_4 again later. Thus we should put one τ_3^{-1} at the beginning of the monodromy and the other τ_3^{-1} at the end. Next, both y_1 and y_2 cross over y_4 so the y_4 term should come next.

It only remains to determine the order of y_1 and y_2, which is given by Table 1 as y_1 then y_2. Therefore our monodromy has the formula $y_3 \circ y_2 \circ y_1 \circ y_4 \circ y_3$, where the first and last y_3 terms are each a τ_3^{-1}. This ordering gives 10 possible crossings, but y_2 and y_3 are parallel and y_3 appears twice. Hence the number reduces to $10 - 3 = 7$, matching the occurrences in Table 2.

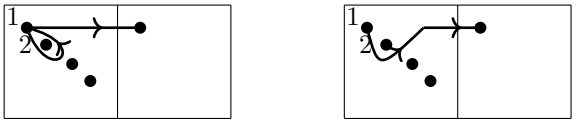

FIGURE 3. C_{12} path in example 1

Piecing all the arguments together shows the final monodromy is isotopic to

$$\tau_3^{-1}\tau_2^{-1}(\tau_1^{-1}\rho_1^{-1}\tau_1^{-1}C_{12})\tau_4^{-1}\rho_4^{-1}\tau_3^{-1} = \tau_3^{-1}\tau_2^{-1}(\tau_1^{-1}\rho_1^{-1}\rho_2^{-1}\tau_1^{-1}\rho_2)\tau_4^{-1}\rho_4^{-1}\tau_3^{-1}.$$

Toroidal example 2. $v_1 = (-1, 1, 1)$.

The paths of the punctures are given by

$$\begin{aligned} y_1(t) &= (-4\epsilon, 3\epsilon) + (0, -1)t, \\ y_2(t) &= (-\epsilon, 2\epsilon) + (1, -2)t, \\ y_3(t) &= (0, 0) + (0, -2)t, \\ y_4(t) &= (\epsilon, -3\epsilon) + (1, -1)t. \end{aligned}$$

Implementing the techniques from the previous example, we obtain the intersections in Table 3. There is only one non-trivial diagonal path, given by y_2. Evaluating this path at the appropriate times yields

$$\begin{aligned} y_2(-3\epsilon) &= (-4\epsilon, 8\epsilon), \\ y_2(\epsilon) &= (0, 0), \\ y_2(2\epsilon) &= (\epsilon, -2\epsilon). \end{aligned}$$

We see that y_2 travels above y_1 and y_4 start points and through y_3 at the origin. We note at $t = \epsilon$, $y_3(\epsilon) = (0, -2\epsilon)$ has traveled away from the origin and so $y_2(t)$ and $y_3(t)$ do not actually collide. Thus, in between $\rho_2^{-1}\rho_2^{-1}\tau_2^{-1}$, we must insert a loop traveling counterclockwise starting at y_2 and enclosing y_1. It turns out this curve is also homotopic to C_{12} (see [1] for more discussion). By drawing a diagram similar to Figure 1 one can see the correct placement should be $\rho_2^{-1}C_{12}\rho_2^{-1}\tau_2^{-1}$. The paths of the other points are straightforward, given by

$$\begin{aligned} &y_1 : \rho_1^{-1}, \\ &y_2 : \rho_2^{-1}C_{12}\rho_2^{-1}\tau_2^{-1} = \rho_2^{-1}\tau_1\rho_2^{-1}\tau_1^{-1}\tau_2^{-1}, \\ &y_3 : \rho_3^{-2}, \\ &y_4 : \tau_4^{-1}\rho_4^{-1}. \end{aligned}$$

The ordering for this example is similar to that of Example 1; this time we need to split both of the paths y_2 and y_4 into two parts each. Notice from the individual monodromies that y_1 and y_3 are parallel so their relative order doesn't matter. We proceed by considering the remaining interactions separately. Since y_1 passes under for all its crossings, it appears first. Then y_3 over y_2 and y_2 over y_4 suggests the ordering $y_3 \circ y_2 \circ y_4$. However, we need y_4 to cross over y_3 and this current arrangement does the opposite. Hence we must split the y_4 monodromy into two components: $y_4 \circ y_3 \circ y_2 \circ y_4$. Finally, if we leave y_2 together, we will have both y_4 and y_2 crossing over one another at different times. Consequently, we also split y_2 for the ultimate ordering given by $y_2 \circ y_4 \circ y_3 \circ y_2 \circ y_4 \circ y_1$. The final monodromy pieces together as

$$y_2 \circ \tau_4^{-1} \circ \rho_3^{-2} \circ y_2 \circ \rho_4^{-1} \circ \rho_1^{-1}.$$

To reiterate, we are required to separate y_2 such that the τ_4^{-1} does not intersect the first term. This obstruction suggests the first y_2 part is τ_2^{-1} and the second term is the remaining $\rho_2^{-1}C_{12}\rho_2^{-1}$. This construction yields the desired map

$$\rho_2^{-1}C_{12}\rho_2^{-1}\tau_4^{-1}\rho_3^{-2}\tau_2^{-1}\rho_4^{-1}\rho_1^{-1}.$$

TABLE 3. Toroidal example 2 intersections

Points	Time	Crossing
(y_2, y_4)	3ϵ	y_2 over y_4
(y_2, y_3)	$\frac{1}{2}$	y_3 over y_2
(y_1, y_4)	$1 - 5\epsilon$	y_4 over y_1
(y_1, y_2)	$1 - 3\epsilon$	y_2 over y_1
(y_3, y_4)	$1 - \epsilon$	y_4 over y_3

Thurston ball revisited. Recall the toroidal examples in Table 1 represent fibrations with fiber a four-times punctured torus. Each such fibration corresponds to an element $\psi \in H^1(T^3, \mathbb{Z})$ on the Thurston ball. We claim ψ must lie in the open cone over a quadrilateral face. This claim follows from [6, Theorem 2.3] and the fact that the fiber has exactly four punctures. Indeed, writing $\psi = (a, b, c)$, we require

$$\begin{aligned}\psi(L_1) &= a = \pm 1,\\ \psi(L_2) &= b = \pm 1,\\ \psi(L_3) &= c = \pm 1,\\ \psi(L_4) &= a + b + c = \pm 1.\end{aligned}$$

These equations yield six possibilities for ψ: $(-1, 1, 1), (1, -1, 1), (1, 1, -1)$, $(-1, -1, 1), (-1, 1, -1)$, $(1, -1, -1)$. Referring to a diagram of the Thurston ball, one can easily verify each of these lives on a quadrilateral face.

5. 4-MANIFOLDS FROM GRAPH LINKS

Here, we study a family of two-component links with different fibrations over a circle, resulting in inequivalent symplectic structures after taking the product with a circle. We start by describing the open 3-manifolds. Let $M^{(2n)} = S^3 \backslash K^{(2n)}$, where $K^{(2n)}$ is the graph link pictured in Figure 4 below. The details of this diagram are given in [10], where the third author showed the existence of $n + 1$ inequivalent symplectic structures coming from different fibrations of $M^{(2n)}$. A fibration of

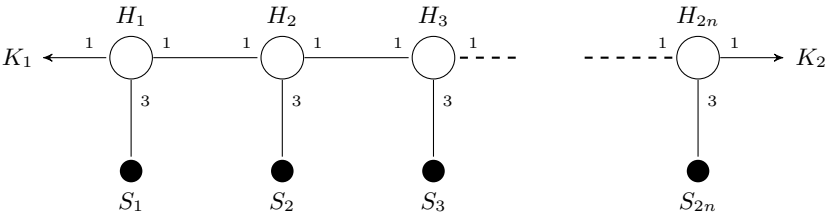

FIGURE 4. Diagram of $K^{(2n)}$

$M^{(2n)}$ is given by a choice of $(m_1, m_2) \in H^1(S^3 \backslash K^{(2n)}), \mathbb{Z}) \cong \mathbb{Z}^2$ satisfying the equations

$$3^i m_1 + 3^{2n-i+1} m_2 \neq 0, \text{ for all } 1 \leq i \leq 2n.$$

Details for such a fibration (and graph link theory in general) are worked out by Eisenbud and Neumann in [3]. In particular, let h denote the monodromy and h_* the induced map on the homology of the fiber. [3, Theorem 13.6] shows that there is an integer q such that $(h_*^q - 1)^2 = 0$. Thus, the Jordan decomposition of h_* only has blocks of size 1 or 2. Furthermore, with the same q, [3] computed the characteristic polynomial of $h_*|_{\mathrm{Im}(h_*^q-1)}$, denoted $\Delta'(t)$. It turns out that the roots of $\Delta'(t)$ correspond to the eigenvalues of h_* with size 2 Jordan blocks. Moreover, the multiplicity of each root λ_i in $\Delta'(t)$ gives the number of size 2 blocks for λ_i.

We first introduce some notation which will be used in the definition of $\Delta'(t)$. Fix a fibration (m_1, m_2). Let $\mathcal{E} = \{E_1, \cdots, E_{2n-1}\}$ be the set of edges connecting the white nodes in Figure 4. Specifically, edge E_i connects nodes labeled H_i and H_{i+1}. For each $E_i \in \mathcal{E}$, we define an integer d_{E_i} as follows. Take the path in $K^{(2n)}$ from the arrowhead of K_1 to halfway through edge E_i (passing through nodes $H_1, H_2, \cdots, H_i$). Let $\ell_{E_i,1}$ denote the product of all weights on edges not contained in the path but are adjacent to vertices in the path. Similarly, we can take the path from the arrowhead of K_2 to halfway through edge E_i and define $\ell_{E_i,2}$ analogously. Set

$$d_{E_i} = \gcd(m_1\ell_{E_i,1}, m_2\ell_{E_i,2}).$$

Using Figure 4 as reference, we can easily compute that $\ell_{E_i,1} = 3^i$ and $\ell_{E_i,2} = 3^{2n-i}$. This simplifies the formula for d_E to

$$d_{E_i} = \gcd(3^i m_1, 3^{2n-i} m_2). \tag{5.1}$$

For each vertex H_i, we define an integer d_{V_i} by the formula

$$d_{V_i} = \begin{cases} \gcd(d_{E_{i-1}}, d_{E_i}), & 1 < i < 2n, \\ \gcd(m_1, d_{E_1}), & i = 1, \\ \gcd(m_2, d_{E_{2n-1}}), & i = 2n. \end{cases} \tag{5.2}$$

With these definitions in place, the (restricted) characteristic polynomial takes the form

$$\Delta'(t) = (t^d - 1) \prod_{i=1}^{2n-1} (t^{d_{E_i}} - 1) / \prod_{i=1}^{2n} (t^{d_{V_i}} - 1),$$

where $d = \gcd(m_1, m_2)$. To understand the details of the theorem to follow, we will use the $n = 2$ case, i.e. $K^{(4)}$, as an illustrative example. Figure 5 demonstrates how $d_{E_1} = \gcd(3m_1, 3^3 m_2)$ is calculated.

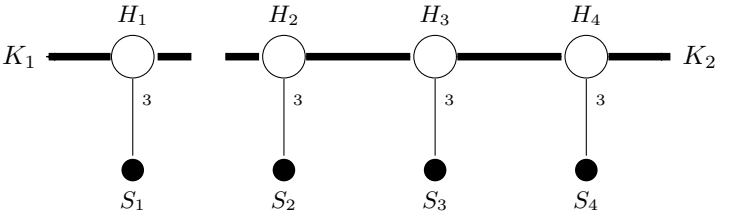

FIGURE 5. Paths $\ell_{E_1,1}$ and $\ell_{E_1,2}$ of d_{E_1}

Now, define $X^{(n)} = S^1 \times M^{(2n)}$ and let $\deg \Delta'(t)$ denote the degree of the restricted characteristic polynomial $\Delta'(t)$. Since $\deg \Delta'(t)$ is the number of Jordan

blocks of size 2, which equals the number of blocks of size *at least* 2, it follows

$$p_2^+ = b_2(X^{(n)}) + 1 + \deg \Delta'(t),$$
$$p_2^- = b_2(X^{(n)}) + \deg \Delta'(t).$$

In the case of a fibration represented by coprime (m_1, m_2), there are two possibilities: 3 divides exactly one of m_1 or m_2, or 3 neither divides m_1 nor m_2. It turns out p_2^+ can distinguish these two possibilities and in the first case provides information about the power of 3 dividing m_1 or m_2. We give the exact statement below.

Theorem 5.1. *Let (m_1, m_2) be coprime, representing a fibration of $M^{(2n)}$. By reversing the roles of m_1 and m_2 if necessary, we write $m_1 = 3^k q$ with $\gcd(q, 3) = 1$ and assume $\gcd(3, m_2) = 1$. It follows that*

$$p_2^+ = \begin{cases} b_2(X^{(n)}) + 3^{n+k-\lceil \frac{k}{2} \rceil} - 3^k, & k \leq 2n-4, \\ b_2(X^{(n)}) + 2 \cdot 3^k, & 2n-3 \leq k \leq 2n-2, \\ b_2(X^{(n)}) + 1, & k \geq 2n-1. \end{cases}$$

Proof. For convenience, we denote by r_k the quantity $\lfloor \frac{2n-k}{2} \rfloor$. Note that r_k is chosen such that $\min(k+i, 2n-i) = k+i$ for $i \leq r_k$. With this fact in mind, we first expand the expressions for d_{E_i}:

$$d_{E_i} = \gcd(3^{k+i} q, 3^{2n-i} m_2) = 3^{\min(k+i, 2n-i)}.$$

A simple consideration shows

$$d_{E_i} = \begin{cases} 3^{k+i}, & i \leq r_k, \\ 3^{2n-i}, & i > r_k. \end{cases}$$

Next, we expand the expressions for V_i. For $1 < i < 2n$, we have

$$d_{V_i} = \gcd(d_{E_{i-1}}, d_{E_i}) = \begin{cases} d_{E_{i-1}}, & i \leq r_k, \\ d_{E_i}, & i > r_k. \end{cases}$$

Verifying the cases where $i \leq r_k$ or $i - 1 > r_k$ is straightforward. For the case $i = r_k + 1$, we have $d_{V_i} = 3^{\min(k+r_k, 2n-r_k-1)}$. A case by case analysis on the parity of k reveals

$$\begin{aligned} r_k &\geq n - \frac{k}{2} - \frac{1}{2} \\ &\implies r_k + r_k \geq 2n - k - 1 \\ &\implies r_k + k \geq 2n - r_k - 1 \end{aligned}$$

and so $d_{V_i} = 3^{2n-r_k-1} = d_{E_{r_{k+1}}} = d_{E_i}$ as required. It remains to compute d_{V_1} and $d_{V_{2n}}$.

$$d_{V_1} = \gcd(m_1, d_{E_1}) = \gcd(3^k q, 3^{\min(k+1, 2n-1)}) = 3^{\min(k, 2n-1)},$$
$$d_{V_{2n}} = \gcd(m_2, d_{E_{2n-1}}) = \gcd(m_2, 3^{\min(k+2n-1, 1)}) = 1,$$

where $d_{V_{2n}}$ follows from the fact that $\gcd(m_2, 3) = 1$. With these definitions, we turn to the formula for $\Delta'(t)$. Its expansion will depend on whether or not there is some index $1 < i < 2n$ for which $i = r_k$. In particular, such an index exists only if $r_k > 1$.

Case 1 ($r_k > 1$). We have

$$\begin{aligned}\Delta'(t) &= \frac{(t-1)(t^{d_{E_1}}-1)\cdots(t^{d_{E_{r_k}}}-1)\cdots(t^{d_{E_{2n-1}}}-1)}{(t^{d_{V_1}}-1)\cdots(t^{d_{V_{r_k}}}-1)\cdots(t^{d_{V_{2n}}}-1)}\\ &= \frac{(t^{d_{E_{r_k}}}-1)}{(t^{d_{V_1}}-1)} = \frac{(t^{3^{k+r_k}}-1)}{(t^{3^{\min(k,2n-1)}}-1)}\\ &= \frac{(t^{3^{k+r_k}}-1)}{(t^{3^k}-1)},\end{aligned}$$

since for $r_k \geq 1$ we have $k < k+1 < 2n-1$.

Case 2 ($r_k \leq 1$). Now we have $d_{E_i} = d_{V_i}$ for all $1 < i < 2n$. Furthermore,

$$d_{E_1} = \begin{cases} 3^{k+1}, & r_k = 1,\\ 3^{2n-1}, & r_k < 1.\end{cases}$$

Recall from the definition of r_k, we also have

$$\min(k, 2n-1) = \begin{cases} k, & r_k = 1,\\ 2n-1, & r_k < 1.\end{cases}$$

Combining the above equalities yields

$$\Delta'(t) = \frac{t^{d_{E_1}}-1}{t^{d_{V_1}}-1} = \frac{t^{d_{E_1}}-1}{t^{3^{\min(k,2n-1)}}-1} = \begin{cases} \frac{t^{3^{k+1}}-1}{t^{3^k}-1}, & r_k = 1,\\ 1, & r_k < 1.\end{cases}$$

To acquire a more straightforward understanding of the three cases $r_k < 1, r_k = 1$, and $r_k > 1$ let us rewrite $r_k = \lfloor \frac{2n-k}{2} \rfloor = n - \lceil \frac{k}{2} \rceil$. Then $r_k = 1$ implies $\lceil \frac{k}{2} \rceil = n-1$ and so $k = 2n-2$ or $2n-3$. Finally, we conclude

$$\deg \Delta'(t) = \begin{cases} 3^{n+k-\lceil \frac{k}{2} \rceil} - 3^k, & k \leq 2n-4,\\ 2 \cdot 3^k, & 2n-3 \leq k \leq 2n-2,\\ 0, & k \geq 2n-1,\end{cases} \tag{5.3}$$

from which the result follows. □

To illustrate some of the details in the proof of Theorem 5.1, we calculate the $K^{(4)}$ case explicitly. Here, we have $r_k = 2 - \lceil \frac{k}{2} \rceil$ and so $r_0 = 2$, $r_1 = r_2 = 1$ and $r_i < 1$ for $i \geq 3$. Note that $r_k \leq 1$ for all $k > 0$. In particular, for $k > 0$ and $i > 1$ we should expect $d_{E_i} = 3^{4-i} = d_{V_i}$. To confirm, we compute

$$\begin{aligned} d_{E_2} &= \gcd(3^{k+2}q, 3^2) = 3^2,\\ d_{E_3} &= \gcd(3^{3+k}q, 3) = 3,\\ d_{V_2} &= \gcd(\min(3^{k+1}, 3^3), 3^2) = \min(3^{k+1}, 3^2) = 3^2,\\ d_{V_3} &= \gcd(3^2, 3) = 3,\\ d_{V_4} &= \gcd(m_2, 3) = 1.\end{aligned}$$

For $i = 1$, we have

$$\begin{aligned} d_{E_1} &= \gcd(3^{k+1}q, 3^3 m_2) = \min(3^{k+1}, 3^3),\\ d_{V_1} &= \gcd(m_1, d_{E_1}) = \gcd(3^k q, 3^{\min(3,k+1)}) = \min(3^3, 3^k).\end{aligned}$$

We can now explicitly compute $\Delta'(t)$:

$$\begin{aligned}\Delta'(t) &= \frac{(t-1)(t^{\min(3^{k+1},3^3)}-1)(t^9-1)(t^3-1)}{(t^{\min(3^k,3^3)}-1)(t^9-1)(t^3-1)(t-1)}\\ &= \frac{t^{3^2\min(3^{k-1},3)}-1}{t^{3\min(3^{k-1},3^2)}-1}\\ &= \begin{cases} t^6+t^3+1, & k=1,\\ t^{18}+t^9+1, & k=2,\\ 1, & k\geq 3.\end{cases}\end{aligned}$$

Indeed, this calculation agrees with the general formula (5.3)

$$\deg(\Delta'(t)) = \begin{cases} 6=2\cdot 3, & k=1,\\ 18=2\cdot 3^2, & k=2,\\ 0, & k\geq 3.\end{cases}$$

We will also use this $K^{(4)}$ example to demonstrate another interesting property of the $X^{(2n)}$ family of open symplectic 4-manifolds. It can be seen in this $n=2$ case that every possible value of p_2^+, in Theorem 5.1, may be achieved for fibrations coming from any of the faces on the Thurston ball. In Figure 6 below, we give the diagram of the Thurston ball for $M^{(4)}$ taken from [10, Figure 3].

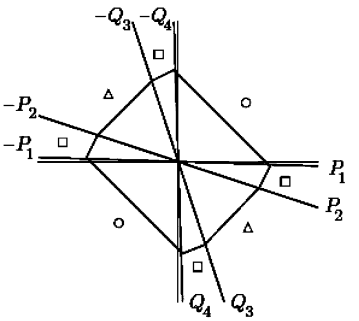

FIGURE 6. Thurston ball for $M^{(4)}$

The eight faces come in three types, denoted by the circular, square, and triangular symbols. The open cone over each face is determined by the rays passing through the primitive elements

$$\begin{aligned}P_i &= (3^{5-2i},-1),\\ Q_i &= (1,-3^{2i-5}).\end{aligned}$$

Consider, for example, the open cone over the circular face in the first quadrant, as the considerations for the other two types of faces are similar. This region is defined by the elements $\{(x,y)|-\frac{1}{27}x<y<27x,\ 0<x<\infty\}$, laying between the P_1 and $-Q_4$ rays. Furthermore, it contains the points $\phi_i=(3^i,1)$ for $0\leq i\leq 3$. By Theorem 5.1, the corresponding symplectic 4-manifolds $(X^{(4)},\omega_i)$ have the following

primitive dimension:

$$p_2^+(X^{(4)}, \omega_1) = b_2 + 9,$$
$$p_2^+(X^{(4)}, \omega_2) = b_2 + 7,$$
$$p_2^+(X^{(4)}, \omega_3) = b_2 + 19,$$
$$p_2^+(X^{(4)}, \omega_4) = b_2 + 1.$$

Moreover, by symmetry of the Thurston ball, the fibrations $-\phi_i$ lie on the cone over the other circular face and also satisfy the above equations. Hence, the pair of circular faces have fibrations with all possible dimensions of p_2^+ given in Theorem 5.1. A similar analysis shows the same property holds true for the square and triangular faces as well.

Since fibrations within a single face of the Thurston ball are all equivalent, i.e. there is a smooth isotopy on the one-form $d\pi$ linking any two fibrations, the above provides examples of symplectic 4-manifolds from equivalent 3-manifold fibrations having different primitive cohomology.

6. Discussion

We conclude with some remarks. Recall from Section 3 that the toroidal and spherical fibrations came from inequivalent faces of the Thurston ball. The cohomological value p_2^+ takes different values for these two types of fibration. The ability to distinguish these two distinct faces in this McMullen-Taubes example arises from the fact that one monodromy is Torelli, while the other is not. In fact, p_2^+ will *always* differ for a Torelli and non-Torelli fibration.

On the other hand, we have also seen from the graph link family of examples that the value of p_2^+ can differ quite a bit for fibrations coming from the *same* face of the Thurston ball. For sure, p_2^+ can give more refined information on each face of the Thurston ball; within a face, p_2^+ can take on different values for various fibrations of X whereas (the classical Betti number) b_2 does not.

It is still however an open question as to how this distinguishing value p_2^+ can be used with other invariants to probe more deeply the relation between different fibrations and their associated symplectic structures. As mentioned, starting with a surface Σ and a monodromy f, we can construct a Y_f and an associated symplectic manifold (X, ω_f). The dimension p_2^+ ultimately comes down to the algebraic structure of the monodromy f on the surface. But as the graph links examples showed, the value of p_2^+ alone is not sufficient in determining which face the monodromy corresponds to. We do expect that the other invariants associated with the underlying A_3-algebra on $PH^*(X, \omega_f)$ [8] will be able to provide even more refined information. The A_3-algebra on the primitive differential forms not only induces a product structure on $PH^*(X, \omega_f)$, but it is also possible to define Massey products on $PH^*(X, \omega_f)$ as well. And as a specific example of how they may provide more information, the triple Massey product can be shown to count the number of Jordan blocks of size exactly three. (See [5] for more information.) It would be interesting to build up a dictionary relating the primitive cohomological invariants of the symplectic 4-manifold with structures on the fibered 3-manifold, and that of the monodromy f, an element of the mapping class group.

Appendix

Here we provide the details of setting up the fibration structure and converting monodromies appropriately so that they can be entered into SnapPy. Let $\mathbb{T}^3$ denote the 3-torus. We view it as the cube $[0,1]^3$ under the identification $(x,y,z) \sim (x+p, y+q, z+r)$ for integers p,q,r. The axes i,j,k and their sum $i+j+k$ form four lines in the cube L_1, L_2, L_3, L_4, respectively. By choosing different bases (v_1, v_2, v_3) for the cube and displacing the four lines we may fiber $\mathbb{T}^3 - \{L_1, L_2, L_3, L_4\}$ in different ways as follows. First we shift the four lines from the origin by

$$\begin{aligned} L_1 &= (x, -\epsilon, 3\epsilon), \\ L_2 &= (\epsilon, y, -3\epsilon), \\ L_3 &= (-\epsilon, \epsilon, z), \\ L_4 &= (x = y = z). \end{aligned}$$

Next we choose a basis $v_1 = (a_1, a_2, a_3)$, $v_2 = (1,1,0)$, $v_3 = (0,1,1)$. Initially v_1 may be any vector which gives a non-zero determinant, specifically, $a_1 - a_2 + a_3 \neq 0$. For brevity, let us denote $A := det(v_1, v_2, v_3) = a_1 - a_2 + a_3$. Choosing to fiber along v_1, each fiber has the form $\Sigma_t = tv_1 + \alpha v_2 + \beta v_3$ for $t \in [0,1]$. Σ_t is $\mathbb{T}^2$ with four punctures denoted $x_1(t), x_2(t), x_3(t), x_4(t)$ coming from the respective lines L_i. To verify that each line L_i intersects the fiber exactly once we must solve the following system of equations:

$$\begin{aligned} L_1 &: \begin{pmatrix} 1 & 1 \\ 0 & 1 \end{pmatrix} \begin{pmatrix} \alpha \\ \beta \end{pmatrix} = \begin{pmatrix} -\epsilon - ta_2 \\ 3\epsilon - ta_3 \end{pmatrix}, \\ L_2 &: \begin{pmatrix} 1 & 0 \\ 0 & 1 \end{pmatrix} \begin{pmatrix} \alpha \\ \beta \end{pmatrix} = \begin{pmatrix} \epsilon - ta_1 \\ -3\epsilon - ta_3 \end{pmatrix}, \\ L_3 &: \begin{pmatrix} 1 & 0 \\ 1 & 1 \end{pmatrix} \begin{pmatrix} \alpha \\ \beta \end{pmatrix} = \begin{pmatrix} -\epsilon - ta_1 \\ \epsilon - ta_2 \end{pmatrix}, \\ L_4 &: \begin{pmatrix} 0 & -1 \\ 1 & -1 \end{pmatrix} \begin{pmatrix} \alpha \\ \beta \end{pmatrix} = \begin{pmatrix} t(a_2 - a_1) \\ t(a_3 - a_1) \end{pmatrix}. \end{aligned}$$

Solving these systems for the (α, β) coordinates of the marked points $x_i(t)$ yields

$$\begin{aligned} x_1(t) &= (-4\epsilon, 3\epsilon) + (a_3 - a_2, -a_3)t, \\ x_2(t) &= (\epsilon, -3\epsilon) + (-a_1, -a_3)t, \\ x_3(t) &= (-\epsilon, 2\epsilon) + (-a_1, a_1 - a_2)t, \\ x_4(t) &= (0,0) + (a_3 - a_2, a_1 - a_2)t. \end{aligned}$$

To align with the notation of [1], we relabel the points with respect to their first coordinate position, in increasing order, as $y_1(t) = x_1(t)$, $y_2(t) = x_3(t)$, $y_3(t) = x_4(t)$, $y_4(t) = x_2(t)$. Under this new setting, the formulas for the points become

$$\begin{aligned} y_1(t) &= (-4\epsilon, 3\epsilon) + (a_3 - a_2, -a_3)t, \\ y_2(t) &= (-\epsilon, 2\epsilon) + (-a_1, a_1 - a_2)t, \\ y_3(t) &= (0,0) + (a_3 - a_2, a_1 - a_2)t, \\ y_4(t) &= (\epsilon, -3\epsilon) + (-a_1, -a_3)t. \end{aligned}$$

Next, we verify that none of the $y_i(t)$ intersect for any value of t. Notice y_2 and y_3 have the same second component in the t variable but differ by the ϵ-term constant so they will never intersect. We can apply a similar argument to the pairs $(y_1, y_3), (y_1, y_4)$, and (y_2, y_4). Lastly, by considering the (separate) systems of equations $y_1(t) = y_2(t)$ and $y_3(t) = y_4(t)$, one can easily see no solution exists.

Let $\Sigma_{1,4}$ be the 2−torus with four punctures and $\mathrm{Mod}(\Sigma_{1,4})$ its mapping class group (which fixes the punctures setwise). Furthermore, let $\mathcal{P}\mathrm{Mod}(\Sigma_{1,4})$ denote the *pure* mapping class group, the set of mapping class elements fixing the punctures pointwise. We set

$$H_1(\Sigma) = \langle a_0, a_1, a_2, a_3, b_0 \rangle, \tag{6.1}$$

where a_i is the homology curve between punctures i and $i+1$ for $i > 0$ and a_0 is between marked point 1 and 4. b_0 is the homology longitudinal curve, not enclosing any punctures. These curves have algebraic intersection numbers $a_i \cdot a_j = 0$ for $i \neq j$ and $a_i \cdot b_0 = 1$. [1] introduces the following elements (pictured below) and shows the Dehn twists along them that generate the pure mapping class group. In our setting we have $\mathcal{P}\mathrm{Mod}(\Sigma_{1,4}) = \langle \mathcal{P}ush(\rho_i), \mathcal{P}ush(\tau_i) \rangle$, $1 \leq i \leq 4$. Here, $\mathcal{P}ush(\gamma)$ is the point pushing map along γ. We also summarize some of the important relations to be used later:

$$\begin{aligned} &[\tau_i, \tau_j] = [\rho_i, \rho_j] = 1, \\ &A_{ij} = \rho_i \tau_j^{-1} \rho_i^{-1} \tau_j, \quad C_{ij} = \tau_i \rho_j^{-1} \tau_i^{-1} \rho_j, \\ &\text{for } 1 \leq i < j < k \leq 4. \end{aligned}$$

For a more in depth discussion and outline of a proof for these identities, see [1].

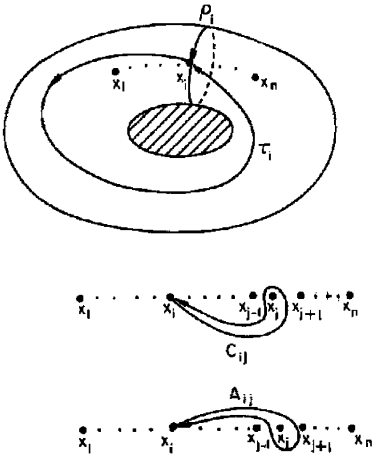

FIGURE 7. Diagram of generators taken from [1]

We note that the formulas here differ slightly from [1] as our choice of orientation is not the same. Moreover, we use functional composition (right to left), as opposed to algebraic. In order to use SnapPy [2], we need to express $\mathcal{P}ush(\rho_i)$ and $\mathcal{P}ush(\tau_i)$ in terms of Dehn twists along the curves in (6.1). The trick is to use the following fact (4.7 proven in [4]), which states

Fact. Let α be a simple loop in a surface S representing an element of $\pi_1(S, x)$, Then $\mathcal{P}ush([\alpha]) = T_a T_b^{-1}$, where a and b are isotopy classes of the simple closed curves in $S - x$ obtained by pushing α off itself to the left and right, respectively.

That is, we take an annular neighborhood of α bounded by curves a and b and then take the product of their Dehn and inverse Dehn twists, respectively. From this construction, we can immediately obtain that

$$\mathcal{P}ush(\rho_i) = T_{a_{i-1}} T_{a_i}^{-1}. \tag{6.2}$$

For the τ_i curves, we need to find an annular boundary to work with. We introduce the longitudinal homology curves b_i, which enclose the punctures $1, 2, \cdots, i$ ["over" $1, 2, \cdots, i$ and "under" $i+1, \cdots, 4$]. Thus b_0 agrees with the previous homology generator introduced, b_1 passes over puncture 1 and misses 2, 3, 4, and so on. The point of introducing these curves is that now τ_i has an annular neighborhood bounded by b_{i-1} and b_i. By consulting the diagrams to determine proper orientation it follows that

$$\mathcal{P}ush(\tau_i) = T_{b_i} T_{b_{i-1}}^{-1}. \tag{6.3}$$

Next, we need to convert equation (6.3) into Dehn twists only involving the homology generators given in (6.1). First, we observe that we may express $[b_i] = [a_0] + [b_0] - [a_i]$, which can be verified by constructing the fundamental square for the torus with the relevant curves. An example diagram in Figure 8 is given for the $[b_1]$ case. One can straightforwardly check that $T_{a_i} T_{b_0}([a_0]) = [a_0] + [b_0] - [a_i] = [b_i]$.

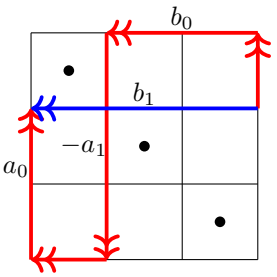

FIGURE 8. Diagram for b_1 expression

Fact 3.7 in [4] states $T_{f(a)} = f T_a f^{-1}$, which we can apply to our situation by setting $a = a_0$ and $f = T_{a_i} T_{b_0}$. This fact then yields

$$T_{b_i} = T_{a_i} T_{b_0} T_{a_0} T_{b_0}^{-1} T_{a_i}^{-1}. \tag{6.4}$$

Finally, substituting formula (6.4) into equation (6.3) leads to our desired expression

$$\mathcal{P}ush(\tau_i) = T_{a_{i-1}} T_{b_0} T_{a_0}^{-1} T_{b_0}^{-1} T_{a_{i-1}}^{-1} T_{a_i} T_{b_0} T_{a_0} T_{b_0}^{-1} T_{a_i}^{-1}. \tag{6.5}$$

ACKNOWLEDGMENTS

We would like to express our thanks to Yi Liu, Curtis McMullen, Yi Ni, Nick Salter, Chung-Jun Tsai, and Jesse Wolfson for helpful conversations.

References

[1] Joan S. Birman, *On braid groups*, Comm. Pure Appl. Math. **22** (1969), 41–72, DOI 10.1002/cpa.3160220104. MR234447

[2] M. Culler, N. M. Dunfield, M. Goerner, and J. R. Weeks, *SnapPy, a computer program for studying the geometry and topology of 3-manifolds*. `http://snappy.computop.org`.

[3] David Eisenbud and Walter Neumann, *Three-dimensional link theory and invariants of plane curve singularities*, Annals of Mathematics Studies, vol. 110, Princeton University Press, Princeton, NJ, 1985. MR817982

[4] Benson Farb and Dan Margalit, *A primer on mapping class groups*, Princeton Mathematical Series, vol. 49, Princeton University Press, Princeton, NJ, 2012. MR2850125

[5] Matthew Gibson, *Properties of the A∞ Structure on Primitive Forms and Its Cohomology*, ProQuest LLC, Ann Arbor, MI, 2019. Thesis (Ph.D.)–University of California, Irvine. MR4051258

[6] Curtis T. McMullen and Clifford H. Taubes, *4-manifolds with inequivalent symplectic forms and 3-manifolds with inequivalent fibrations*, Math. Res. Lett. **6** (1999), no. 5-6, 681–696, DOI 10.4310/MRL.1999.v6.n6.a8. MR1739225

[7] Walter D. Neumann, *Splicing algebraic links*, Complex analytic singularities, Adv. Stud. Pure Math., vol. 8, North-Holland, Amsterdam, 1987, pp. 349–361, DOI 10.2969/aspm/00810349. MR894301

[8] Chung-Jun Tsai, Li-Sheng Tseng, and Shing-Tung Yau, *Cohomology and Hodge theory on symplectic manifolds: III*, J. Differential Geom. **103** (2016), no. 1, 83–143. MR3488131

[9] Li-Sheng Tseng and Shing-Tung Yau, *Cohomology and Hodge theory on symplectic manifolds: II*, J. Differential Geom. **91** (2012), no. 3, 417–443. MR2981844

[10] Stefano Vidussi, *Homotopy K3's with several symplectic structures*, Geom. Topol. **5** (2001), 267–285, DOI 10.2140/gt.2001.5.267. MR1825663

[11] Stefano Vidussi, *Smooth structure of some symplectic surfaces*, Michigan Math. J. **49** (2001), no. 2, 325–330, DOI 10.1307/mmj/1008719776. MR1852306

Department of Mathematics, University of California, Irvine, California 92697
Email address: `gibsonmd@uci.edu`

Department of Mathematics, University of California, Irvine, California 92697
Email address: `lstseng@math.uci.edu`

Department of Mathematics, University of California, Riverside, California 92521
Email address: `svidussi@ucr.edu`